V International Conference on Computational Methods for Coupled Problems in Science and Engineering
COUPLED PROBLEMS 2013
S. Idelsohn, M. Papadrakakis and B. Schrefler (Eds)

NUMERICAL SIMULATION OF INDUCTIVE HEATING PROCESSES

T. GLEIM, D. KUHL AND B. SCHRÖDER*

Institute of Mechanics and Dynamics
University of Kassel
Mönchebergstrae 7, 34109 Kassel, Germany
e-mail: kuhl@uni-kassel.de, web page: http://www.uni-kassel.de/fb14/mechanics

Key words: finite element method, heat equation, heat induction, MAXWELL equations

Abstract. For product optimization regarding weight reduction, material properties have to be adapted efficiently. To achieve this, new compositions of materials can be created or the manufacturing process can be changed in a way that heterogeneous distributions of material properties are enabled. An example for such an improved process chain is the production of thermo-mechanically graded structures like shafts. The manufacturing method mainly consists of three stages. The first one is characterized by a local temperature increase of the workpiece due to inductive heating. In the second phase the workpiece is deformed and simultaneously cooled throughout the contact with the forming die. In the last step, however, a high pressured air stream is applied, leading to a partial cooling of the workpiece.
The inductive heating step is controlled by an alternating current inducing a high frequency magnetic field, which causes a temperature increase due to the resulting eddy currents. To analyse this process, the coupling between the electric and the magnetic field is described by the fully coupled MAXWELL equations. Moreover the heat conduction equation is considered to describe thermal effects. To solve this multifield the equations are in the first step decoupled using an additional time differentiation. In the second step an axisymmetric case is considered, motivated by the fact that the inductive heating process of a cylindrical shaft is analysed. Afterwards the resulting equations are spatially discretized by the GALERKIN finite element method. The temporal discretization is carried out via the NEWMARK method so that afterwards the electrical source distribution can be achieved. As a consequence the temperature evolution is determined in a postprocessing step.

1 INTRODUCTION

In order to optimize material properties, new material composites or new fabrication sequences are developed. An example for the latter mentioned aspect is a thermo-

mechanical forming process, where locally varying material properties are achieved due to heterogenous temperature fields during the manufacturing process. As an illustration the production of a shaft within an integrated fabrication process is treated. The first step consists of an inductive heating, afterwards the shaft is formed as well as cooled due to the contact with the forming die and in the end a cold pressured air stream is applied, compare Figure 1.

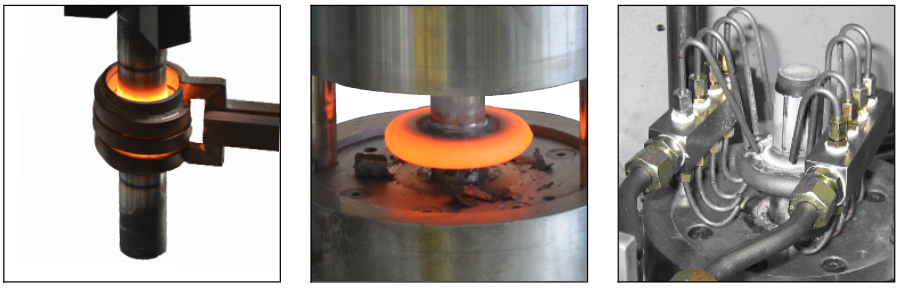

Figure 1: Thermomechanical forming process with inductive heating [6]

The inductive heating step is an essential part of the production sequence, since due to this a material gradiation is enabled and the forming process is facilitated. Thus this process step will be analyzed in what follows solving the coupled MAXWELL equations using a finite element spatial discretization and a time discretization.

2 MAXWELL EQUATIONS AND CONSTITUTIVE ASSUMPTIONS

To describe electromagnetic phenomena mathematically, for instance that magnetic sources do not exist (2), the MAXWELL equations

$$\nabla \cdot \boldsymbol{D} = \rho_R \tag{1}$$

$$\nabla \cdot \boldsymbol{B} = 0 \tag{2}$$

$$\nabla \times \boldsymbol{H} = \boldsymbol{J} + \dot{\boldsymbol{D}} \tag{3}$$

$$\nabla \times \boldsymbol{E} = -\dot{\boldsymbol{B}} \tag{4}$$

are used. Herein $\boldsymbol{B}$ denotes the magnetic and $\boldsymbol{D}$ the electric flux density. Moreover, $\boldsymbol{H}$ as well as $\boldsymbol{E}$ are called magnetic and electric field intensity, respectively. The variable $\boldsymbol{J}$ represents the electric current density and ρ_R the electric charge density.
Nevertheless not all variables included in the MAXWELL equations are independent of each other, thus they are linked, assuming the following constitutive equations, [3].

$$\boldsymbol{D} = \epsilon \boldsymbol{E} \tag{5}$$

$$\boldsymbol{B} = \mu \boldsymbol{H} \tag{6}$$

$$\boldsymbol{J} = \sigma \boldsymbol{E} + \boldsymbol{J}_{\mathrm{i}} \tag{7}$$

Herein

$$\epsilon = \epsilon_0 \epsilon_\mathrm{R} \tag{8}$$

represents the permittivity, consisting of the electric permittivity in the vacuum ϵ_0 and a material dependent part ϵ_R. Likewise the variable

$$\mu = \mu_0 \mu_\mathrm{R} \tag{9}$$

embodies the permeability. The constant σ symbolizes the electric conductivity and the variable $\boldsymbol{J}_\mathrm{i}$ the intrinsic current density.
Having a closer look on the equations above the basis of an inductive heating process can be explained. In general in an inductive heating process the workpiece is surrounded by an induction coil, on which an alternating current is applied, [5]. In accordance with equation (3) this alternating current $\boldsymbol{J}$ produces an alternating magnetic field, which is, following equation (4) and (7), the source of induced eddy currents in the workpiece. If in addition the heat equation

$$\rho\sigma c\dot{\Theta} + \sigma\nabla\cdot\boldsymbol{q} \;=\; \boldsymbol{J}^2 \tag{10}$$

with the the heat capacity c, the density ρ and the constitutive equation

$$\boldsymbol{q} \;=\; -\lambda\nabla\Theta \tag{11}$$

connecting the heat flux vector $\boldsymbol{q}$ with the temperature Θ throughout the heat conduction coefficient λ, is considered, then it can be followed that these eddy currents are the reason for the temperature increase in the workpiece. Since the equations for the inductive heating process are now all known, the next chapter will show one possible solution strategy, [1].

3 AXISYMMETRIC FORMULATION

The following analysis is motivated by the inductive heating of a shaft with the help of an induction coil. Both of this parts can be considered as axisymmetric domains, so that instead of using a three-dimensional model an axisymmetric formulation considering cylindrical coordinates (r, ϕ, z) is used. Thus a meridian half-plane of the shaft and the induction coil, described by the coordinates (r, z) and setting $\phi = const.$, is observed, compare Figure 2. Before this assumption is exploited further, the Maxwell equations are reformulated. Therefore, the constitutive laws (5) as well as (6) are inserted in equation (3)

$$\nabla\times\frac{1}{\mu}\boldsymbol{B} = \boldsymbol{J} + \epsilon\dot{\boldsymbol{E}}. \tag{12}$$

The resulting relation is time differentiated and equation (4) is furthermore considered. This leads to

$$\sigma\frac{\partial\boldsymbol{E}}{\partial t} + \epsilon\frac{\partial^2\boldsymbol{E}}{\partial t^2} + \frac{1}{\mu}\nabla\times\nabla\times\boldsymbol{E} \;=\; -\frac{\partial\boldsymbol{J}_\mathrm{i}}{\partial t}. \tag{13}$$

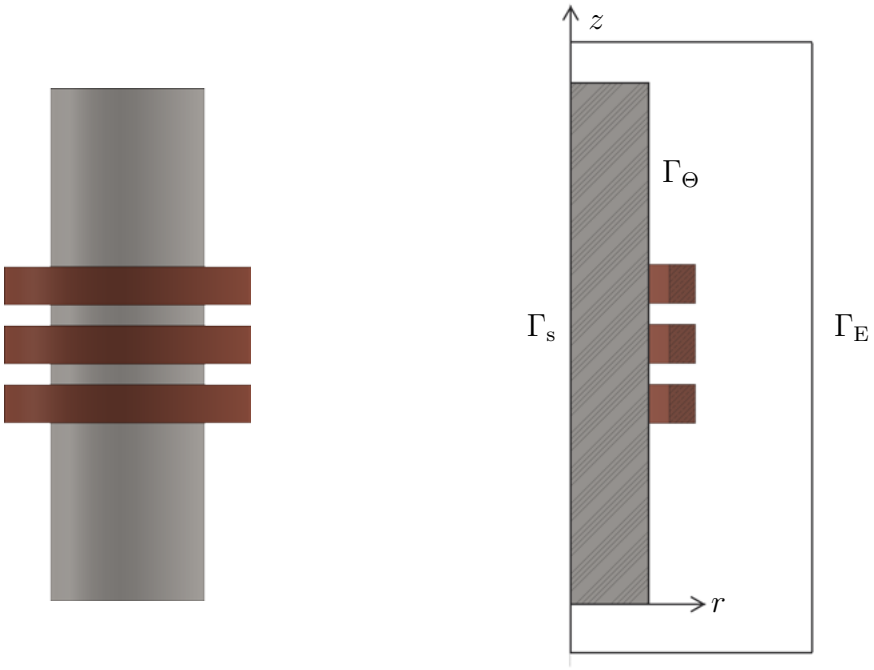

Figure 2: Shaft with induction coil

An analogous treatment of equation (4) results in a similar relation

$$\epsilon \frac{\partial^2 \boldsymbol{B}}{\partial t^2} + \frac{1}{\mu} \nabla \times \nabla \times \boldsymbol{B} \;=\; \nabla \times \boldsymbol{J}. \tag{14}$$

The other two MAXWELL equations (1) as well as (2) are not affected and stay unaltered. Thus by considering geometric aspects in the framework of an axisymmetric formulation a decoupling of AMPERÉ'S (3) and FARADAY'S law (4) is achieved, if in addition the current density $\boldsymbol{J}$ is known and adequate initial conditions are assumed, [2]. On the explicit formulation of the initial conditions as well as of the boundary conditions will be commented later on.
Since the aim is to describe the temperature evolution, moreover, just the electric equation (13) together with the heat equation (10) are considered and their weak forms are generated.

3.1 WEAK FORM OF THE ELECTRIC FIELD EQUATION AND THE HEAT EQUATION

To enable the usage of the Finite Element Method, partial differential equations have to be formulated weakly throughout a multiplication with a test function i.e. $\delta \boldsymbol{E}$ or $\delta\Theta$ and an integration over a volume Ω. For the electric field evolution equation and the temperature evolution equation this leads to:

$$\int_\Omega \sigma\delta\boldsymbol{E}\cdot\dot{\boldsymbol{E}}\,dV+\int_\Omega \epsilon\delta\boldsymbol{E}\cdot\ddot{\boldsymbol{E}}\,dV+\frac{1}{\mu}\int_\Omega \delta\boldsymbol{E}\cdot\nabla\times\nabla\times\boldsymbol{E}\,dV+\int_\Omega \delta\boldsymbol{E}\cdot\dot{\boldsymbol{J}}_{\mathrm{i}}\,dV = 0 \quad (15)$$

$$\int_\Omega \delta\Theta\,\sigma\rho c\dot{\Theta}\,dV+\int_\Omega \delta\Theta\,\sigma\nabla\cdot\boldsymbol{q}\,dV-\int_\Omega \delta\Theta\,\boldsymbol{J}^2\,dV = 0 \quad (16)$$

Using Green's formula

$$\int_\Omega \delta\boldsymbol{E}\cdot\nabla\times\nabla\times\boldsymbol{E}\,dV=\int_\Omega \nabla\times\delta\boldsymbol{E}\cdot\nabla\times\boldsymbol{E}\,dV+\int_\Gamma \delta\boldsymbol{E}\cdot\boldsymbol{n}\times\nabla\times\boldsymbol{E}\,dA \quad (17)$$

and the divergence theorem, equations (15) and (16) can be determined to

$$\begin{aligned}\int_\Omega \sigma\delta\boldsymbol{E}\cdot\dot{\boldsymbol{E}}\,dV &+ \int_\Omega \epsilon\delta\boldsymbol{E}\cdot\ddot{\boldsymbol{E}}\,dV+\frac{1}{\mu}\int_\Omega \nabla\times\delta\boldsymbol{E}\cdot\nabla\times\boldsymbol{E}\,dV+ \\ &+ \frac{1}{\mu}\int_\Gamma \delta\boldsymbol{E}\cdot\boldsymbol{n}\times\nabla\times\boldsymbol{E}\,dA+\int_\Omega \delta\boldsymbol{E}\cdot\dot{\boldsymbol{J}}_{\mathrm{i}}\,dV = 0\end{aligned} \quad (18)$$

$$\int_\Omega \delta\Theta\,\sigma\rho c\dot{\Theta}\,dV-\int_\Omega \delta\nabla\Theta\,\sigma\cdot\boldsymbol{q}\,dV+\int_\Gamma \delta\Theta\boldsymbol{q}\cdot\boldsymbol{n}\,dA-\int_\Omega \delta\Theta\,\boldsymbol{J}^2\,dV=0 \quad (19)$$

3.2 SPATIAL DISCRETIZATION

Due to the spatial discretization the whole domain Ω is divided into several finite elements and the continuous field variables are described with the help of discrete node values and shape functions. For this, standard Lagrange functions N^i are employed, [7].

$$\boldsymbol{E}^{\mathrm{e}}\approx\sum_{i=1}^{NN}\boldsymbol{E}^{\mathrm{e}i}N^i \qquad \Theta^{\mathrm{e}}\approx\sum_{i=1}^{NN}\Theta^{\mathrm{e}i}N^i \quad (20)$$

$$\ddot{\boldsymbol{E}}^{\mathrm{e}}\approx\sum_{i=1}^{NN}\ddot{\boldsymbol{E}}^{\mathrm{e}i}N^i \qquad \dot{\Theta}^{\mathrm{e}}\approx\sum_{i=1}^{NN}\dot{\Theta}^{\mathrm{e}i}N^i \quad (21)$$

$$\delta\boldsymbol{E}^{\mathrm{e}}\approx\sum_{i=1}^{NN}\delta\boldsymbol{E}^{\mathrm{e}i}N^i \qquad \delta\Theta^{\mathrm{e}}\approx\sum_{i=1}^{NN}\delta\Theta^{\mathrm{e}i}N^i \quad (22)$$

If further the geometrical aspect is considered, that the current density $\boldsymbol{J}$ has just a component in $\boldsymbol{e}_\phi$ direction, then the spatial discretized weak forms result in

$$\sum_{i=1}^{NN}\sum_{j=1}^{NN}\delta E^{\mathrm{e}i}\epsilon\int_{\Omega_\mathrm{e}} N^i N^j \ddot{E}^{\mathrm{e}j} r dr dz + \frac{\delta E^{\mathrm{e}i}}{\mu}\int_{\Omega_\mathrm{e}}\left[\frac{\partial N^i}{\partial z}\frac{\partial N^j}{\partial z} + \frac{1}{r^2}\frac{\partial\left(rN^i\right)}{\partial r}\frac{\partial\left(rN^j\right)}{\partial r}\right]E^{\mathrm{e}j} r dr dz \quad (23)$$
$$+ \ \delta E^{\mathrm{e}i}\int_{\Omega_\mathrm{e}} N^i \dot{J}_\mathrm{i} r dr dz + \delta E^{\mathrm{e}i}\sigma\int_{\Omega_\mathrm{e}} N^i N^j \dot{E}^{\mathrm{e}j} r dr dz = 0$$

$$\sum_{i=1}^{NN}\sum_{j=1}^{NN}\delta\Theta^{\mathrm{e}i}\int_{\Omega_\mathrm{e}}\rho c\sigma\dot{\Theta}^{\mathrm{e}j} N^i r dr dz + \sigma\lambda\delta\Theta^{\mathrm{e}i}\int_{\Omega_\mathrm{e}}\left[\frac{\partial N^i}{\partial r}\frac{\partial N^j}{\partial r} + \frac{\partial N^i}{\partial z}\frac{\partial N^j}{\partial z}\right] r dr dz + \quad (24)$$
$$+ \ \delta\Theta^{\mathrm{e}i}\int_{\Omega_\mathrm{e}} J^2 N^i r dr dz = 0$$

for each element. To get the above listed equations, adequate boundary conditions have to be exploited. For the electric field this is fulfilled by setting

$$E = 0 \qquad \text{on} \quad \Gamma_\mathrm{s}\cup\Gamma_\mathrm{E}. \quad (25)$$

For the boundary Γ_s this represents a symmetry condition, whereas on the the rest of Γ_E the influence of the electric field is neglected. The boundary condition for the temperature evolution equation is

$$\boldsymbol{q}\cdot\boldsymbol{n} = 0 \qquad \text{on} \quad \Gamma_\Theta. \quad (26)$$

If all elements are assembled to the desired structure and matrix notations are used, then equations (24) and (25) result in

$$\boldsymbol{M}\ \ddot{\boldsymbol{E}} + \boldsymbol{D}_\mathrm{E}\ \dot{\boldsymbol{E}} + \boldsymbol{K}_\mathrm{E}\ \boldsymbol{E} + \boldsymbol{r}_\mathrm{E} = \boldsymbol{0} \quad (27)$$
$$\boldsymbol{D}_\Theta\ \dot{\boldsymbol{\Theta}} + \boldsymbol{K}_\Theta\ \boldsymbol{\Theta} + \boldsymbol{r}_\Theta = \boldsymbol{0}. \quad (28)$$

Moreover these equations have to be discretized temporarily.

3.3 TEMPORAL DISCRETIZATION

In a first step the time interval $[0,T]$ with the time step Δt is examined using as a time discretization the Generalized-α method, [4], with $\alpha_\mathrm{m} = \alpha_\mathrm{f} = 0.5$

$$\dot{\boldsymbol{E}}_{n+\frac{1}{2}} = \frac{1}{2}\left[\frac{\gamma}{\beta\Delta t}\left[\boldsymbol{E}_{n+1} - \boldsymbol{E}_n\right] - \frac{\gamma-\beta}{\beta}\dot{\boldsymbol{E}}_n + \dot{\boldsymbol{E}}_n\right] \quad (29)$$
$$\ddot{\boldsymbol{E}}_{n+\frac{1}{2}} = \frac{1}{2}\left[\frac{1}{\beta\Delta t^2}\left[\boldsymbol{E}_{n+1} - \boldsymbol{E}_n\right] - \frac{1}{\beta\Delta t}\dot{\boldsymbol{E}}_n - \frac{1-2\beta}{2\beta}\ddot{\boldsymbol{E}}_n + \ddot{\boldsymbol{E}}_n\right] \quad (30)$$
$$\dot{\boldsymbol{\Theta}}_{n+\frac{1}{2}} = \frac{1}{2}\left[\frac{\gamma}{\beta\Delta t}\left[\Theta_{n+1} - \Theta_n\right] - \frac{\gamma-\beta}{\beta}\dot{\Theta}_n + \dot{\Theta}_n\right], \quad (31)$$

assuming $2\beta = \gamma = \frac{1}{2}$ and considering

$$\dot{\boldsymbol{E}}(t_0) = \dot{\boldsymbol{E}}_0 \qquad \boldsymbol{E}(t_0)=\boldsymbol{E}_0 \tag{32}$$

$$\Theta(t_0) = \Theta_0 \tag{33}$$

as appropriate initial conditions. Inserting the above mentioned formulations leads to two linear systems of equations

$$\hat{\boldsymbol{K}}_{\mathrm{E}}\ \boldsymbol{E} \ = \ \hat{\boldsymbol{r}}_{\mathrm{E}}\left(\ddot{\boldsymbol{E}}_n, \dot{\boldsymbol{E}}_n, \boldsymbol{E}_n\right) \tag{34}$$

$$\hat{\boldsymbol{K}}_{\Theta}\ \boldsymbol{\Theta} \ = \ \hat{\boldsymbol{r}}_{\Theta}\left(\dot{\Theta}_n, \Theta_n\right), \tag{35}$$

which can be solved in two steps. In the first step the electric field equation is solved, determining the current density $\boldsymbol{J}$ at each node. Afterwards the temperature evolution equation is solved in a postprocessing step, containing the current density $\boldsymbol{J}$ as prescribed load vector and determining the temperature field.
Since now the theoretical aspects are explained in the next chapter a simulated inductive heating process is described.

4 NUMERICAL EXAMPLE

As a numerical example for the above deduced theory the inductive heating process of the shaft, see Figure 2, with three rings as induction coil will be examined. Therefor a sinusoidal current with a current I and a frequency f will be applied to each of the induction rings. Then the evolution of the electric field and the temperature field will be calculated. The necessary material parameters and load factors are listed in the table below.

Table 1: Materialparameters and loads

μ_{Rshaft}	μ_{Rcoil}	$\epsilon_{\mathrm{Rshaft}}$	$\epsilon_{\mathrm{Rcoil}}$	σ	λ	c	I	f
$600\ \frac{\mathrm{Vs}}{\mathrm{Am}}$	$1\ \frac{\mathrm{Vs}}{\mathrm{Am}}$	$0\ \frac{\mathrm{As}}{\mathrm{Vm}}$	$1\ \frac{\mathrm{As}}{\mathrm{Vm}}$	$10^6\ \frac{1}{\Omega\mathrm{m}}$	$39,88\ \frac{\mathrm{W}}{\mathrm{mK}}$	$620\ \frac{\mathrm{Nm}}{\mathrm{kgK}}$	5000A	8100 Hz

The following figures, compare Figure 3, are achieved for the electrical as well as for the temperature field. It can be seen that with increasing distance r from the shaft the influence of the electrical field decreases. Moreover, the three induction rings cause a symmetric distribution of the electric field inside the shaft with a very small induction depth. At the interface between shaft and air an unsteady electric field is noticeable, which is explicable due to the different material properties.
For the calculation of the temperature field only the shaft itself was considered and the influence of the surrounding air was neglected. The temperature field distribution is symmetric but in contrast to the electric field distribution not only the periphery is affected. The whole shaft, at the height of the induction coils, is heated up.

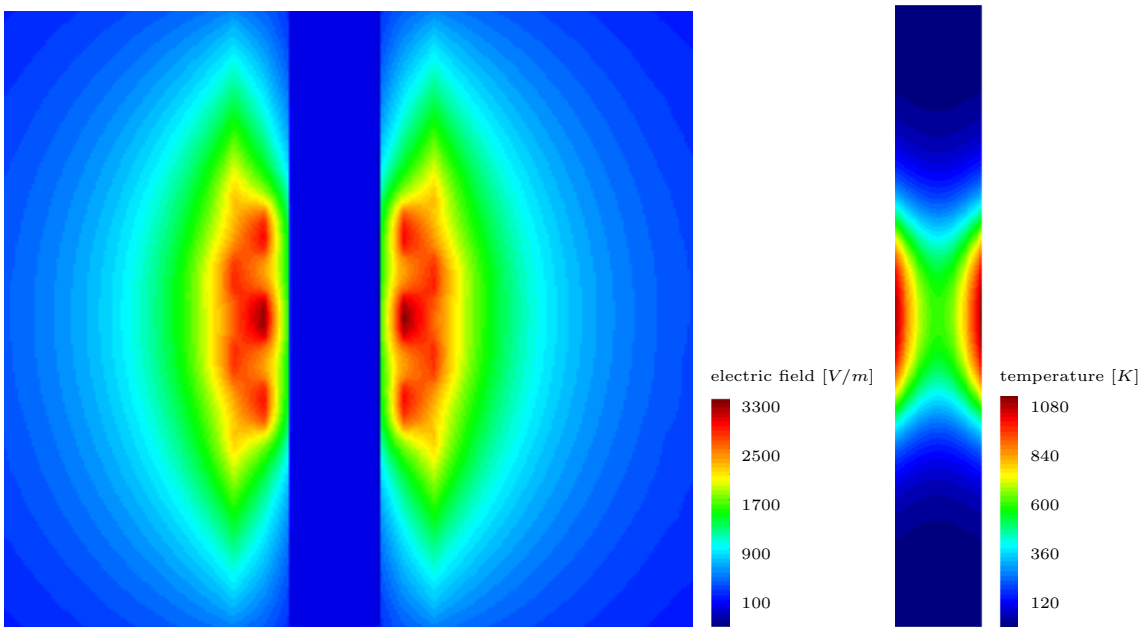

Figure 3: Segment of electrical field intensity (left) and temperature field (right)

5 CONCLUSION AND OUTLOOK

In this paper a method is shown to determine the temperature field during an inductive heating process. Therefore the MAXWELL equations are used to derive an axisymmetric formulation for the electric field intensity, whose solution enables the determination of the current density distribution. Furthermore, in a postprocessing step, the heat equation is solved, considering the current density as heat source.
To achieve the before mentioned, first the weak form of the electric field intensity equation as well as the weak form of the temperature evolution equation has to be generated. Then the finite element method is used as spatial discretization and the generalized-α method is carried out as temporal discretization. Afterwards linear systems of equations are solved and moreover, the realization is demonstrated.
In the next step a monolithic scheme should be developed to solve the electrical field equation and the heat equation at the same time. This approach towards a nonlinear system of equations will make it possible to consider temperature dependent material properties.

6 ACKNOWLEDGEMENT

Financial support was provided by the German National Science Foundation (DFG) in the framework of project C1 of the collaborative research center (SFB/TR TRR 30). This support is gratefully acknowledged.

REFERENCES

[1] Assous, F., Ciarlet, P., Labrunie, S. and Segré, J. Numerical solution to the time-dependent Maxwell equations in axisymmetric singular domains: the singular complement method *Journal of Computational Physics.*(2003). **191**:147-176.

[2] Assous, F., Degond, P., Heintze, E., Raviart, P.A. and Segré, J. On a Finite-Element Method for Solving the Three-Dimensional Maxwell Equations *Journal of Computational Physics.*(1993). **109**:222-237.

[3] Beck, R., Deuflhard, P., Hiptmair, R., Hopper, R.H.W. and Wohlmuth, B. Adaptive multilevel methods for edge element discretizations of Maxwell's equations *Surveys of Mathematics for industry.*(1995)

[4] Chung, J. and Hulburt, G.M. A time integration algorithm for structural dynamics with improved numerical dissipation: The generalized-α method *Journal of Applied Mechanics.*(1993). **60**:371-375.

[5] Rudnev, V., Loveless, D., Cook, R. and Black, M. *Handbook of Induction Heating.* Marcel Dekker Inc (2003).

[6] Steinhoff, K., Weidig, U. and Saba, N. Investigation of plastic forming under the influence of locally and temporally variable temperature and stress states. Steinhoff, K., Maier, H. and Biermann, D., editors, *Functionally Graded Materials in Industrial Mass production*, 35-52. Verlag Wissenschaftliche Scripten.

[7] Zienkiewicz, O.C. and Taylor, R.L. *The FINITE ELEMENT METHOD.* Butterworth Heinemann (2000), Volume I.